RSC Advances

PAPER

View Article Online
View Journal | View Issue

Cite this: *RSC Adv.*, 2015, **5**, 21237

Hierarchical TiO_2 spheres decorated with Au nanoparticles for visible light hydrogen production†

Guoqiang Zhang,[ab] Zhao Zhao,[ab] Huaqiao Tan,[a] Haifeng Zhao,[a] Dan Qu,[ab] Min Zheng,[a] Weixing Yu*[c] and Zaicheng Sun*[a]

Received 5th December 2014
Accepted 18th February 2015

DOI: 10.1039/c4ra15818k

www.rsc.org/advances

Hierarchical TiO_2 spheres composed of nanosheets are successfully synthesized *via* a simple solvothermal route. TiO_2 spheres with high surface area (~100 m^2 g^{-1}) exhibit excellent photocatalytic activity. Au nanoparticles are loaded on the surface of TiO_2 nanosheets through anchor molecules – thiolglycolic acid. The LSPR absorption band at ~550 nm of Au nanoparticles is clearly observed in the diffusion reflective UV-Vis spectra. H_2 production results show that the TiO_2 spheres have higher photocatalytic activity than commercial P25 TiO_2. After loading with Au nanoparticles, TiO_2–Au spheres display a 27.6 μmol (g^{-1} h^{-1}) H_2 production rate under visible light irradiation (λ > 420 nm) because the localized surface plasmon resonance (LSPR) of Au nanoparticles enhances the visible light absorption. Furthermore, the H_2 production rate could be improved to 92.4 μmol (g^{-1} h^{-1}) for TiO_2 spheres loaded with both Au and Pt nanoparticles. Based on these results, we propose a possible mechanism. Under UV light, TiO_2 absorbs UV light and generates excited electrons, passing to Au nanoparticles for H_2 production. In the case of visible light irradiation, the hot electrons are generated from Au nanoparticles due to the LSPR effect. And then the hot electrons are transferred from the Au nanoparticles to TiO_2 and cocatalyst Pt nanoparticles for H_2 generation.

Introduction

Titanium dioxide (titania, TiO_2) is one of the most widely used semiconducting oxide materials and has a wide range of applications including bio-separation, sensors, energy storage, solar cells, catalysis and photocatalysis.[1–7] TiO_2 offers a number of advantageous characteristics including low cost, relatively high photocatalytic activity, low toxicity, and high chemical and optical stability. Since the discovery of hydrogen production from water through electrochemical photolysis,[8] TiO_2 has been intensively studied and used as a photocatalyst in both fundamental research and practical applications.[9–11] Due to its large band gap (E_g = 3.0–3.2 eV), it can absorb UV light and generate electron (e^-) and hole (h^+) pairs which can induce a variety of redox reactions. Over the past few decades, tremendous efforts have been devoted to improving the catalytic activity of TiO_2-based photocatalysts with well controlled characteristics.[12–14] However, weak absorption in visible region lies still on the way for the practical applications like solar water splitting. Generally, a few routes have been used for improving the absorption of TiO_2 in visible region. Firstly, doping TiO_2 with metal (like Fe^{3+}, Cr^{3+}, Ti^{3+} *etc.*) or non-metal (for example C, N, S and so on) will narrow the band gap.[11,15–18] Secondly, sensitizing TiO_2 with narrow band gap quantum dots or dye molecules, which absorb visible light and inject electron or hole into TiO_2, improves the overall photocatalytic capability of TiO_2.[19–23]

Another promising route to enhance the photocatalytic performance of TiO_2 is to decorate the surface with noble metal nanoparticles (*e.g.* Ag, Au, Pt, and Pd).[24–28] It has been shown that the presence of the noble metal nanoparticles can effectively shift the Fermi level of TiO_2, which results in the enhanced photocatalytic efficiency.[24,29] On the other hand, the localized surface plasmon resonance (LSPR) of noble metal nanoparticles also enhances the absorption in the visible region of TiO_2. Kamat *et al.* investigated the size dependence of Au–TiO_2 nanocomposites and found that small Au particles lead to large apparent Fermi level shift (20 mV for 8 nm diameter and 40 mV for 5 nm and 60 mV for 3 nm gold nanoparticles), which improves the photoinduced charge separation.[24] In traditional way, adding the noble metal salt into TiO_2 sol–gel precursor and photo-reducing the noble metal salts, it is hard to avoid the aggregation of gold nanoparticle to form big particles.[30–32] Preparation of TiO_2 hierarchical nanostructures loaded with Au

[a]*State Key Laboratory of Luminescence and Applications, Changchun Institute of Optics, Fine Mechanics and Physics, Changchun, 130033, Jilin, P. R. China. E-mail: sunzc@ciomp.ac.cn*

[b]*University of Chinese Academy of Sciences, Beijing, P. R. China*

[c]*Insititue of Micro and Nano Optics, College of Optoelectronic Engineering, Shenzhen University, Shenzhen 518060, China*

† Electronic supplementary information (ESI) available: More SEM, EDAX, H_2 production of TiO_2 spheres. See DOI: 10.1039/c4ra15818k

nanoparticles are highly desired. Recently, Lou *et al.* reported the hierarchical TiO_2 spheres composed in nanosheets with high surface area ($\sim$100 m^2 g^{-1}) and high reactive (001) facet.[33] On the other hand, this hierarchical TiO_2 spheres have both accessible macropores from intersheets and mesopores from the packing of nanoparticles within nanosheets.

Herein, hierarchical TiO_2 spheres composed in nanosheets were synthesized *via* modified Lou's route. Based on the hierarchical TiO_2 spheres, we developed a facile method to load Au nanoparticles on the surface of TiO_2 nanosheets by introducing an anchor molecule thioglycolique acid (TGA), which effectively controls the size of Au nanoparticles with $\sim$5 nm in diameter. The obtained TiO_2–Au spheres possess the following advantages: (i) hierarchical structure shows high photocatalytic performance from large surface area; (ii) the LSPR of Au nanoparticles enhances the visible light absorption and improves the photocatalytic performance of TiO_2 in the visible light region. H_2 production experiments indicate that the TiO_2–Au spheres show a high photocatalytic performance in both UV and visible region due to Au nanoparticles on the TiO_2 surface. That makes TiO_2 spheres decorated with Au nanoparticles as a high active visible-light photocatalyst.

Results and discussion

Firstly, the large scale of TiO_2 spheres were prepared according to Lou's report with a modification.[33] Fig. S1† shows field-emission scanning electron microscopy (FE-SEM) images of the obtained TiO_2 spheres, which size can be tuned from 400–800 nm in diameter by reaction conditions. Close inspection images disclose that the TiO_2 spheres are composed of TiO_2 nanosheets, which is about 10 nm in thickness. High resolution TEM image displays that the nanosheets are composed of TiO_2 nanoparticles with $\sim$6 nm of diameter after long time calcination. The crystalline phase of these TiO_2 spheres can be transferred into anatase phase under calcination at 400 °C for 2–4 hours. The XRD patterns as shown in Fig. 3A, the calcined TiO_2 spheres exhibit a typical anatase crystalline phase pattern (JCPDS no. 21-1272). To obtain Au nanoparticles on the TiO_2 nanosheets surface, here we used an anchor molecule TGA, which has two functional groups, carboxyl group (–COOH) and thiol group (–SH). The COOH group makes the anchor molecules attach on the TiO_2 surface. The thiol group on the other side will expose on the surface. Au complexes (Au (TGA)) forms between TGA and $HAuCl_4$ with the addition of $HAuCl_4$. Then Au nanoparticles form by adding into fresh $NaBH_4$ solution. The anchor molecule TGA has a key role for the Au nanoparticles formation. It can effectively prevent from the aggregation of Au.

Fig. 1 show the FE-SEM images of TiO_2 spheres decorated with Au nanoparticles. After loading Au nanoparticles, the morphology of TiO_2 spheres is well kept. With the increase of $HAuCl_4$ amount, the more $HAuCl_4$ can be adsorbed on the TGA modified surface of TiO_2 spheres. After reducing, Au nanoparticles are denser on the surface of TiO_2 spheres. The energy dispersive X-ray analysis (EDAX, Fig. S2 and S3†) proves the existence of Au. According to EDAX results, the weight fraction of loaded Au nanoparticles increases from 1.07, 2.00, 2.43 to 2.82 wt% by adding 5, 10, 20 and 30 mL of 1.0 mmol L^{-1} $HAuCl_4 \cdot 3H_2O$ solution into TiO_2 sphere dispersion for samples TiO_2–Au1, 2, 3, and 4, respectively. Fig. 2 display transmission electron microscopy (TEM) images of TiO_2 spheres decorated with Au nanoparticles. Low magnification TEM image (Fig. 2A) clearly shows the TiO_2 sphere with nanosheets structures. High resolution TEM images exhibit that 0.35 and 0.24 nm are characteristic lattice fringe space of anatase TiO_2 (101) and Au

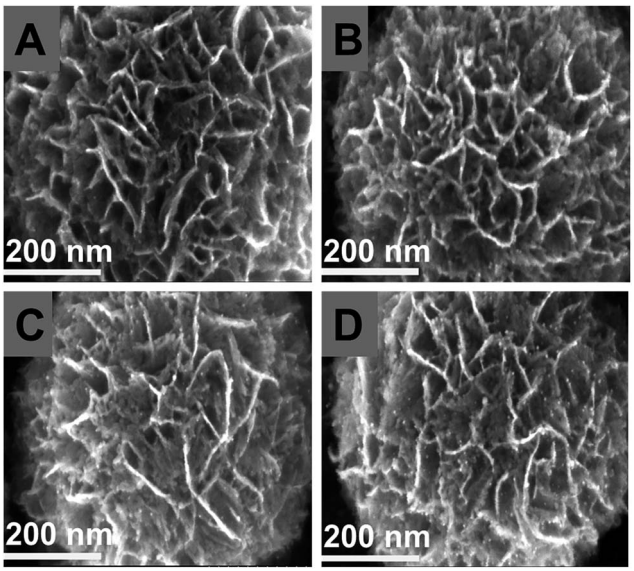

Fig. 1 Field emission scanning electron microscopy (FE-SEM) images of TiO_2 spheres decorated with different amount of Au nanoparticles. (A) 1.07 wt% (TiO_2–Au1), (B) 2.00 wt% (TiO_2–Au2), (C) 2.43 wt% (TiO_2–Au3) and (D) 2.82 wt% (TiO_2–Au4) measured from EDAX.

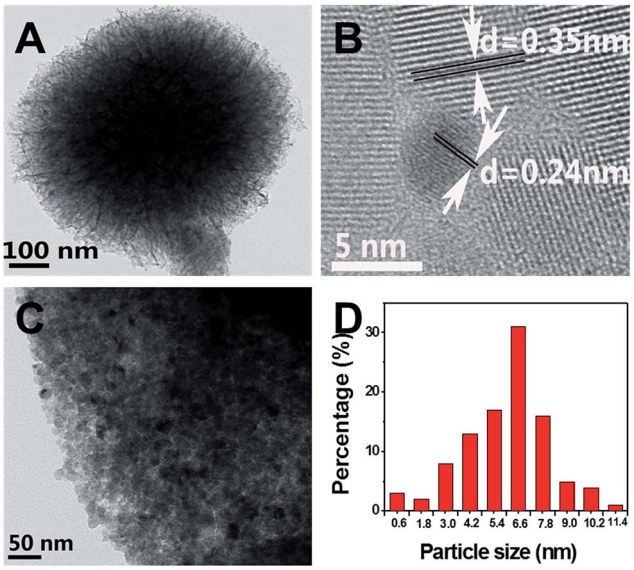

Fig. 2 Transmission electron microscopy (TEM) images of TiO_2 spheres loaded with 2.43 wt% Au nanoparticles (A and C). (B) is the high resolution TEM image of TiO_2 loaded with Au nanoparticles. 0.35 nm and 0.24 nm are characteristic lattice fringe space of anatase TiO_2 (101) and Au (111) nanoparticles. The histogram of TiO_2 nanoparticles calculated from TEM images of (C).

(111) nanoparticles, respectively. That reveals the uniform Au nanoparticles with ~5 nm in diameter are attached on the TiO_2 nanosheets. In addition, the TiO_2 nanosheets are composed of TiO_2 nanoparticles with diameter of 6.01 ± 1.61 nm (Fig. 2C and D).

Fig. 3A displays the X-ray diffraction patterns of TiO_2 loaded with different amount of Au nanoparticles. It clearly shows the diffraction peaks at 25.3, 37.8, 48.0 degree, which are related to the (101), (004), (200) of anatase phase TiO_2 (JCPDS no. 21-1272). According to the Scherrer equation, the TiO_2 nanocrystal size was calculated to be 10 nm using (101) reflection peak. It is consistent with the diameter of TiO_2 measured from TEM images. Diffused reflective UV-Vis spectroscopy is presented in the Fig. 3B. Compared with TiO_2 spheres, a broad absorption band at ~550 nm, related to the plasmon resonance of Au, is observed for the TiO_2 spheres loaded with Au nanoparticles. The hierarchical TiO_2 spheres exhibit high surface area. The Brunauer–Emmett–Teller (BET) surface area and pore size of the TiO_2 spheres are characterized using nitrogen adsorption–desorption isotherm shown in Fig. 3C and D. It gives a type-IV isotherm with a type-H3 hysteresis loop, indicating a mesoporous structure.[34] The BET surface area of TiO_2 spheres with and without Au nanoparticles are determined to be 97 and 103 $m^2\ g^{-1}$, respectively. According to previous reports,[35] a bimodal mesopore size distribution was implied in this type of hysteresis loop. The hysteresis loop in the lower relative pressure range ($0.4 < P/P_0 < 0.8$) is attributed to the mesopores from the packing of nanoparticles within nanosheets and that in the high relative pressure range ($0.8 < P/P_0 < 1.0$) is related to the macropores from intersheets.

TiO_2 spheres exhibit high photocatalytic activity compared with commercial P25 TiO_2. Fig. S4A† shows the H_2 production of TiO_2 spheres and P25 TiO_2 loaded with 1 wt% Pt as cocatalyst under UV-Vis light (300 W Xe lamp). The H_2 evolution rate is about 335 and 204 μmol $hour^{-1}$ for 10 mg TiO_2 sphere and P25 TiO_2, respectively. The main reason is that TiO_2 spheres have larger surface area than P25 TiO_2 (~50 $m^2\ g^{-1}$). No H_2 production is observed for 10 mg of TiO_2 sphere under UV-visible light (Fig S4B†). It exhibits obvious photocatalytic activity after loading Au nanoparticles. The H_2 production rate is ~23.9, 53.6, 165 and 87.3 μmol $hour^{-1}$ for 10 mg sample of TiO_2–Au1, 2, 3, and 4, respectively. The photocatalytic activity reaches maximum when the Au nanoparticles amount is about 2.43 wt% (TiO_2–Au3). These results indicate that Au nanoparticles could work as a cocatalyst for H_2 production. TiO_2 adsorbs UV light and the electron was excited from valance band (VB) to conduction band (CB), then the photogenerated electron can inject into Au nanoparticles. The proton accepts the electron and forms H_2.

Fig. 4 shows H_2 production rate of TiO_2 sphere with different amount Au nanoparticles under visible light (λ > 420 nm) in presence and absence of Pt cocatalyst. No H_2 is produced from the pure TiO_2 sphere without loading Au nanoparticles. That indicates that TiO_2 spheres have no response to the visible light. Fig. S5† shows TiO_2 spheres loaded both Au and Pt nanoparticles. When Au nanoparticles are attached onto the TiO_2 sphere surface, H_2 is detected. That means that Au nanoparticles absorb the visible light, generate hot electron due to the LSPR effect and transfer hot electron to TiO_2 for H_2 generation. The H_2 evolution rate increases with the increasing of Au nanoparticles amount. However, too much amount of Au nanoparticles (2.84 wt%) results in a decrease of H_2 production rate. The optimal loading amount of Au nanoparticles is about 2.43 wt% and H_2 production rate is about 27 μmol ($g^{-1}\ h^{-1}$). Pt is often chosen as a cocatalyst to lower the over potential of H_2O splitting. Furthermore, when the cocatalyst Pt nanoparticles are loaded onto the TiO_2–Au spheres *via* photo-reduction reaction,

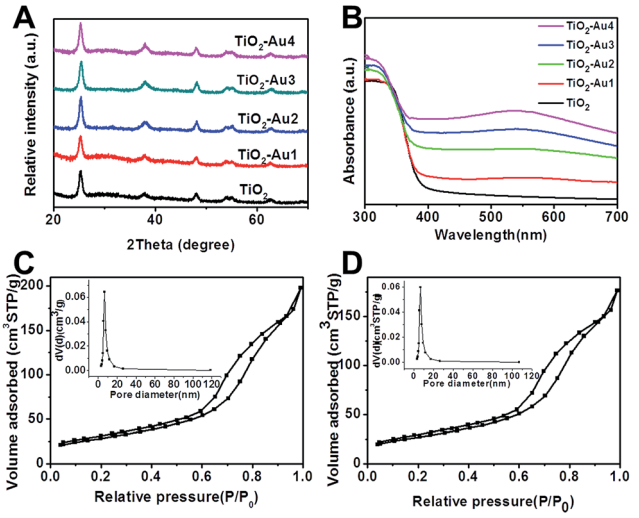

Fig. 3 X-ray diffraction pattern (A) and diffusion reflection UV-Vis spectra (B) of TiO_2 spheres loaded different amount of Au nanoparticles (TiO_2–Au1–4 for Au weight fraction 1.07, 2.00, 2.43, 2.82 wt% respectively). (C and D) are the N_2 sorption curves of TiO_2 sphere without and with Au nanoparticles, respectively. Insets are the pore size distribution curves.

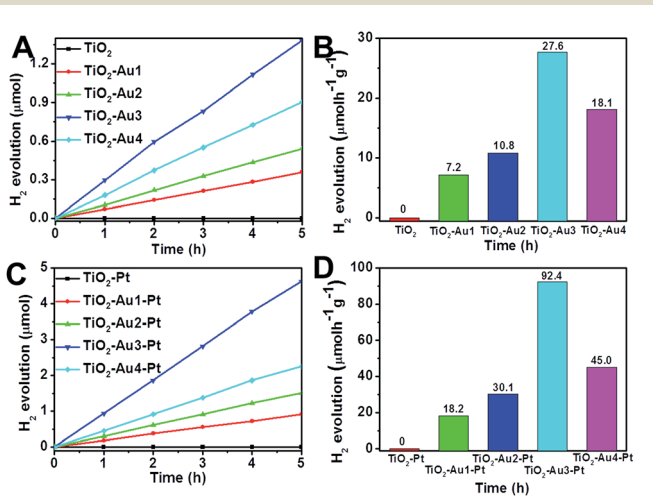

Fig. 4 (A) H_2 production of TiO_2 spheres loaded with different amount Au nanoparticles under visible light (λ > 420 nm). (B) Normalized H_2 production rate of TiO_2 sphere with Au nanoparticles. (C) H_2 production of TiO_2 spheres loaded with Au and Pt nanoparticles under visible light (λ > 420 nm). (D) Normalized H_2 production rate of TiO_2 spheres loaded Au and Pt nanoparticles.

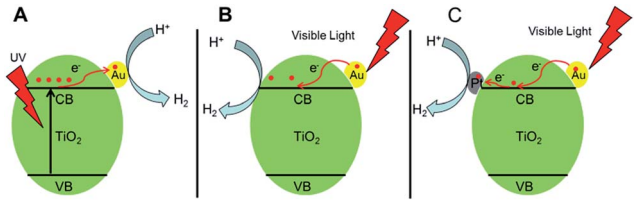

Scheme 1 Possible photocatalytic H_2 production mechanism of TiO_2–Au under full spectrum light (A) and visible light (λ > 420 nm), where B is TiO_2–Au and C is TiO_2–Au and Pt nanoparticles.

the H_2 production rate has obvious improvement. The H_2 production rate increases from 27 μmol (g^{-1} h^{-1}) to 92 μmol (g^{-1} h^{-1}), which is about 3 folds improvement.

Based on the above results, we propose the following mechanism for TiO_2–Au composites (Scheme 1). Under UV light illumination, TiO_2 adsorbs light and is excited to generate exciton. The electron is transferred to Au nanoparticles, which work as cocatalyst to promote H_2 generation (Scheme 1A). It is known that a Schottky barrier is formed at the Au–TiO_2 interface when Au nanoparticles make direct physical contact with TiO_2.[36] Upon excitation of the Au SPR with λ > 420 nm, intense SPR-enhanced EM field are generated on the surface of Au nanoparticles, increasing the yield of interfacial "hot electrons". That will induce efficient transfer of "hot electrons" to the CB of TiO_2. The Schottky barrier at the interface also helps the transferred "hot electrons" accumulating in the TiO_2 CB, preventing them from traveling back to Au nanoparticles. Since no holes are generated in the valence band (VB) of TiO_2 under λ > 435 nm excitation, the transferred "hot electrons" in the TiO_2 CB should have much longer lifetimes, fostering the reduction of H_2O to produce H_2.[37,38] Further, the reduction of H_2O is promoted by the loading of cocatalyst Pt nanoparticle. The "hot electron" is transferred from Au nanoparticle to the CB of TiO_2, then further to the Pt nanoparticles. Pt nanoparticles prefer to adsorb the proton and lower the over potential of H_2O reduction.[39] The hot electrons prefer transfer from Au nanoparticles to Pt nanoparticles where hydrogen evolution occurs. That is the reason why H_2 production rate has an obvious improvement after loading Pt nanoparticles.

Conclusions

In summary, we have loaded Au nanoparticles on the surface of TiO_2 spheres through anchor molecules thiolglycolic acid. SEM and TEM disclosed that Au nanoparticles are well dispersed on the surface of TiO_2 sphere. Due to TiO_2 spheres are composed of nanosheets, it possesses relatively large surface area (~100 m^2 g^{-1}), which is beneficial to the photocatalytic performance. TiO_2 spheres exhibit high photocatalytic H_2 production rate (165 μmol $hour^{-1}$ for 10 mg of TiO_2–Au3) under full spectrum light. The TiO_2 spheres loaded with Au nanoparticles also shows good photocatalytic activity under visible light illumination due to the LSPR effect of Au nanoparticles. The photocatalytic performance could be further improved to 97 μmol $hour^{-1}$ for 10 mg TiO_2–Au3 by loading the cocatalyst Pt nanoparticle on the TiO_2.

Experimental

Chemicals and materials

$HAuCl_4 \cdot 3H_2O$ (AR), $NaBH_4$ (98%), thioglycolic acid (TGA, AR, 90%), diethylenetriamine (DETA, 99%), and titanium isopropylate (TIP, 98%) were purchased from Aladdin Reagent Company. Methanol (AR), isopropanol (AR) was purchased from Beijing Chemical Reagent Company. All chemicals were used without any further purification.

Synthesis of TiO_2 sphere

At room temperature, the 380 mL of isopropanol was mixed with 300 L of DETA and stirred for 30 min. Then the 12.5 mL of TIP was injected with mixture slowly. The above solution was transferred into a 500 mL Teflon lined stainless steel autoclave and was heated to 200 °C for 48 h in an electric oven. Following this, the reaction was naturally cooled to room temperature. The as-prepared samples were washed with ethanol to remove remaining organic impurity and dried at 70 °C for 12 h in an electric oven. Finally, the samples were annealed at 400 °C for 4 h to form the crystal phase of TiO_2.

Synthesis of TiO_2–Au

At room temperature, the 80 mg of TiO_2 sphere was dispersed into 10 mL of deionized water. 100 μL of TGA was added into the mixture and stirred for 6 h to make TGA adsorb on TiO_2 sphere surface. Then the above mixture was centrifuged at 9000 rpm for 15 min to remove free TGA molecules. Then, 5, 10, 20 and 30 mL of 1.0 mmol L^{-1} $HAuCl_4 \cdot 3H_2O$ solution was added into TiO_2 spheres dispersion and stirred for 6 h away from light to make gold ion bonded with TGA. Then the mixture was centrifuged at 9000 rpm for 15 min to remove free gold ion. 5 mL of 0.1 mol L^{-1} $NaBH_4$ solution was injected rapidly and stirred at 1000 rpm. The as-prepared samples were centrifuged and washed with deionized water. Finally, the samples were dried at 70 °C for 12 h.

Characterizations

The Brunauer–Emmett–Teller (BET) specific surface area was measured using a Micromeritics Gemini V Surface Area and Pore Size Analyzer. Scanning electron microscope (SEM) images were measured on JEOL JSM 4800F. Transmission electron microscope (TEM) images were taken using an FEI Tecnai G2 operated at 200 kV. The UV-Vis absorption spectra were recorded on a UV-3600 UV-Vis-NIR scanning spectrophotometer (Shimadzu). The crystalline structure was recorded by using an X-ray diffractometer (XRD) (Bruker AXS D8 Focus), using Cu K_α radiation (λ = 1.54056 Å).

Photocatalytic activity measurements

10 mg of TiO_2–Au photocatalyst was placed into an aqueous methanol solution (120 mL, 25 vol%) in a closed gas circulation system (Perfect Light Company Labsolar-III (AG)). The UV-visible light irradiations were obtained from a 300 W Xe lamp (Perfect Light Company Solaredge 700) without and with a

UVCUT-420 nm filter (CE Aulight. Inc). The evolved gases were detected *in situ* by using an online gas chromatograph. (GC-2014C, Shimadzu) equipped with a thermal conductivity detector (TCD). To obtain TiO_2–Au–Pt photocatalyst, 10 mg of TiO_2–Au photocatalyst loaded with 1.0 wt% Pt (H_2PtCl_6) was placed into an aqueous methanol solution in a closed gas circulation system. Before collecting the evolution gas, the reaction was irradiated with UV-Vis light over an hour for reduction Pt nanoparticles onto the TiO_2–Au samples.

Acknowledgements

The authors thank the National Natural Science Foundation of China (no. 21301166, 21201159, and 61361166004), Science and Technology Department of Jilin Province (no. 20130522127JH, and 20121801) are gratefully acknowledged. Z. S. thanks the support of the "Hundred Talent Program" of CAS. Supported by open research fund program of State Key Laboratory of Luminescence and Applications (CIOMP, CAS) and Key Laboratory of Functional Inorganic Material Chemistry (Heilongjiang University), Ministry of Education, P. R. China.

Notes and references

1 X. Chen and S. S. Mao, *Chem. Rev.*, 2007, **107**, 2891–2959.
2 M. Graetzel, R. A. J. Janssen, D. B. Mitzi and E. H. Sargent, *Nature*, 2012, **488**, 304–312.
3 J. Du, J. Qi, D. Wang and Z. Tang, *Energy Environ. Sci.*, 2012, **5**, 6914–6918.
4 K. Nakata and A. Fujishima, *J. Photochem. Photobiol., C*, 2012, **13**, 169–189.
5 Q. Zhang, E. Uchaker, S. L. Candelaria and G. Cao, *Chem. Soc. Rev.*, 2013, **42**, 3127–3171.
6 T. Froschl, U. Hormann, P. Kubiak, G. Kucerova, M. Pfanzelt, C. K. Weiss, R. J. Behm, N. Husing, U. Kaiser, K. Landfester and M. Wohlfahrt-Mehrens, *Chem. Soc. Rev.*, 2012, **41**, 5313–5360.
7 H. G. Moon, Y.-S. Shim, H. W. Jang, J.-S. Kim, K. J. Choi, C.-Y. Kang, J.-W. Choi, H.-H. Park and S.-J. Yoon, *Sens. Actuators, B*, 2010, **149**, 116–121.
8 A. Fujishima and K. Honda, *Nature*, 1972, **238**, 37–38.
9 X. Chen, S. Shen, L. Guo and S. S. Mao, *Chem. Rev.*, 2010, **110**, 6503–6570.
10 X. Chen, L. Liu, P. Y. Yu and S. S. Mao, *Science*, 2011, **331**, 746–750.
11 F. Zuo, K. Bozhilov, R. J. Dillon, L. Wang, P. Smith, X. Zhao, C. Bardeen and P. Feng, *Angew. Chem., Int. Ed.*, 2012, **51**, 6223–6226.
12 J. Lee, M. Christopher Orilall, S. C. Warren, M. Kamperman, F. J. DiSalvo and U. Wiesner, *Nat. Mater.*, 2008, **7**, 222–228.
13 M. Yin, Y. Cheng, M. Liu, J. S. Gutmann and K. Müllen, *Angew. Chem., Int. Ed.*, 2008, **47**, 8400–8403.
14 H. G. Yang, C. H. Sun, S. Z. Qiao, J. Zou, G. Liu, S. C. Smith, H. M. Cheng and G. Q. Lu, *Nature*, 2008, **453**, 638–641.
15 W. Choi, A. Termin and M. R. Hoffmann, *J. Phys. Chem.*, 1994, **98**, 13669–13679.
16 E. Borgarello, J. Kiwi, M. Graetzel, E. Pelizzetti and M. Visca, *J. Am. Chem. Soc.*, 1982, **104**, 2996–3002.
17 R. Asahi, T. Morikawa, T. Ohwaki, K. Aoki and Y. Taga, *Science*, 2001, **293**, 269–271.
18 D. Pan, J. Zhang, Z. Li, C. Wu, X. Yan and M. Wu, *Chem. Commun.*, 2010, **46**, 3681–3683.
19 D. R. Baker and P. V. Kamat, *Adv. Funct. Mater.*, 2009, **19**, 805–811.
20 H. Park, W. Choi and M. R. Hoffmann, *J. Mater. Chem.*, 2008, **18**, 2379–2385.
21 C. Karakaya, Y. Türker and Ö. Dag, *Adv. Funct. Mater.*, 2013, **23**, 4002–4010.
22 E. Bae and W. Choi, *Environ. Sci. Technol.*, 2002, **37**, 147–152.
23 *Sustainable Nanotechnology and the Environment: Advances and Achievements*, ed. N. Shamim and K. Sharma Virender, American Chemical Society, 2013.
24 V. Subramanian, E. E. Wolf and P. V. Kamat, *J. Am. Chem. Soc.*, 2004, **126**, 4943–4950.
25 Y. Lai, Y. Tang, J. Gong, D. Gong, L. Chi, C. Lin and Z. Chen, *J. Mater. Chem.*, 2012, **22**, 7420–7426.
26 R. Su, R. Tiruvalam, Q. He, N. Dimitratos, L. Kesavan, C. Hammond, J. A. Lopez-Sanchez, R. Bechstein, C. J. Kiely, G. J. Hutchings and F. Besenbacher, *ACS Nano*, 2012, **6**, 6284–6292.
27 H. Li, Z. Bian, J. Zhu, Y. Huo, H. Li and Y. Lu, *J. Am. Chem. Soc.*, 2007, **129**, 4538–4539.
28 C. Zhou, L. Shang, H. Yu, T. Bian, L.-Z. Wu, C.-H. Tung and T. Zhang, *Catal. Today*, 2014, **225**, 158–163.
29 K. Mogyorósi, Á. Kmetykó, N. Czirbus, G. Veréb, P. Sipos and A. Dombi, *React. Kinet. Catal. Lett.*, 2009, **98**, 215–225.
30 M. Epifani, C. Giannini, L. Tapfer and L. Vasanelli, *J. Am. Ceram. Soc.*, 2000, **83**, 2385–2393.
31 S. C. Chan and M. A. Barteau, *Langmuir*, 2005, **21**, 5588–5595.
32 X. Z. Li and F. B. Li, *Environ. Sci. Technol.*, 2001, **35**, 2381–2387.
33 J. S. Chen, Y. L. Tan, C. M. Li, Y. L. Cheah, D. Luan, S. Madhavi, F. Y. C. Boey, L. A. Archer and X. W. Lou, *J. Am. Chem. Soc.*, 2010, **132**, 6124–6130.
34 M. Kruk and M. Jaroniec, *Chem. Mater.*, 2001, **13**, 3169–3183.
35 K. Kaneko, *J. Membr. Sci.*, 1994, **96**, 59–89.
36 Y. K. Lee, C. H. Jung, J. Park, H. Seo, G. A. Somorjai and J. Y. Park, *Nano Lett.*, 2011, **11**, 4251–4255.
37 J. S. DuChene, B. C. Sweeny, A. C. Johnston-Peck, D. Su, E. A. Stach and W. D. Wei, *Angew. Chem., Int. Ed.*, 2014, **53**, 7887–7891.
38 K. Qian, B. C. Sweeny, A. C. Johnston-Peck, W. Niu, J. O. Graham, J. S. DuChene, J. Qiu, Y.-C. Wang, M. H. Engelhard, D. Su, E. A. Stach and W. D. Wei, *J. Am. Chem. Soc.*, 2014, **136**, 9842–9845.
39 D. Duonghong, E. Borgarello and M. Graetzel, *J. Am. Chem. Soc.*, 1981, **103**, 4685–4690.